Comparisons of the transmitted signals of time, aperture, and angle gating in biological tissues and a phantom

Yih-Ming Wang, Chia-Wei Sun, Cheng-Kuan Lee, Chih-Wei Lu, Meng-Tsan Tsai, C. C. Yang, and Yean-Woei Kiang

Graduate Institute of Electro-Optical Engineering, Graduate Institute of Communication Engineering and Department of Electrical Engineering, National Taiwan University, 1, Roosevelt Road, Sec. 4, Taipei, Taiwan, R.O.C.
ccy@cc.ee.ntu.edu.tw

Abstract: We measure transmitted signals with time, aperture, and angle gating for comparison in micro-sphere suspension, chicken breast and chicken liver tissues. We find that in each sample, the small aperture-gated (angle-gated) signals for imaging are essentially different from those of early time gating. Meanwhile, the signals obtained from aperture and angle gating come from quite different parts of the transmitted photons. For biological tissues of different structures, different gating methods may lead to different levels of imaging quality. Also, the results indicate the generally different scattering characteristics of biological tissues from that of a particle-based phantom. The scattering nature in the biological tissues may imply that random continuum scattering needs to be considered in biological imaging. Between chicken breast and liver tissues, the time-gated data show that the later has stronger scattering and absorption.

OCIS codes: (170.0170) Medical optics and biotechnology; (170.3660) Light propagation in tissues; (290. 5850) Scattering, particles.

References and links

1. D. Huang, E. A. Swanson, C. P. Lin. J. S. Schuman, W. G. Stinson, W. Chang, M. R. Hee, T. Flotte, K. Gregory, C. A. Puliafito, J. G. Fujimoto, "Optical Coherence Tomography," Science **254**, 1178 (1991).
2. K. M. Yoo, B. B. Das, and R. R. Alfano, "Imaging of a transluncent object hidden in a highly scattering medium from the early portion of the diffuse component of a transmitted ultrafast laser pulse," Opt. Lett. **17**, 958 (1992).
3. L. Wang, P. P. Ho, and R. R. Alfano**, "**Time-resolved Fourier spectrum and imaging in highly scattering media," Appl. Opt. **32**, 5043 (1993).
4. L. Wang, X. Liang, P. Galland, P. P. Ho, and R. R. Alfano, "True scattering coefficients of turbid matter measured by early-time gating," Opt. Lett. **20**, 913 (1995).
5. S. G. Demos and R. R. Alfano, "Temporal gating in highly scattering media by the degree of optical polarization," Opt. Lett. **21**, 161 (1996).
6. X. D. Zhu, Sung-po Wei, Shechao Charles Feng, and Britton Chance, "Analysis of a diffuse-photon-density wave in multiple-scattering media in the presence of a small spherical object," J. Opt. Soc. Am. A **13**, 494 (1996).
7. J. Ripoll, M. Nieto-Vesperinas, and mi Carminat, "Spatial resolution of diffuse photon density waves," J. Opt. Soc. Am. A **16**, 1466 (1999).
8. Yu Chen, Chenpeng Mu, Xavier Intes, and Britton Chance, "Adaptive calibration for object localization in turbid media with interfering diffuse photon density waves," Appl. Opt. **41**, 7325 (2002).
9. Steven P. Schilders, Xiaosong S. Gan, and Min Gu, "Microscopic imaging through a turbid medium by use of annular objectives for angle gating," Appl. Opt. **37**, 5320 (1998).
10. Adam Wax, Changhuei Yang, Ramachandra R. Dasari, and Michael S. Feld, "Measurement of angular distributions by use of low-coherence interferometry for light-scattering spectroscopy," Opt. Lett. **26**, 322 (2001).
11. Koichi Shimizu and Masataka Kitama, "Fundamental study on near-axis scattered light and its application to optical computed tomography," Opt. Rev. **7**, 383 (2000).

#3820 - $15.00 US Received 13 February 2004; revised 9 March 2004; accepted 16 March 2004

12. Hsiang-Hsu Wang, Chia-Wei Sun, Yih-Ming Wang, Yean-Woei Kiang, and C. C. Yang, "Determination of the depth of a scattering target in a turbid medium with polarization discrimination of transmitted signals," Opt. Lett. **28**, 25 (2003).
13. Chia-Wei Sun, Chih-Yu Wang, C. C. Yang, Yean-Woei Kiang, I-Jen Hsu, and Chii-Wann Lin, "Polarization gating in ultrafast-optics imaging of skeletal muscle tissues," Opt. Lett. **26**, 432 (2001).
14. Chia-Wei Sun, Kuei-Chao Liu, Yih-Ming Wang, Hsiang-Hsu Wang, Yean-Woei Kiang, Hua-Kuang Liu, and C. C. Yang, "Determination of target depth in a turbid medium with polarization-dependent transmitted signals," J. Opt. Soc. Am. A **20**, 2106 (2003).
15. Steven P. Schilders, Xiaosong S. Gan, and Min Gu, "Resolution improvement in microscopic imaging through turbid media based on differential polarization gating," Appl. Opt. **37**, 4300 (1998).
16. Gilbert Jarry, Elisa Steimer, Vivien Damaschini, Michael Epifanie, Marc Jurczak, Robin Kaiser, "Coherence and polarization of light propagating through scattering media and biological tissues," Appl. Opt. **37**, 7357 (1998).
17. Vanitha Sankaran, Matthew J. Everett, Duncan J. Maitland, and Joseph T. Walsh, Jr., "Comparison of polarized-light propagation in biological tissue and phantoms," Opt. Lett. **24**, 1044 (1999).
18. Vanitha Sankaran, Joseph T. Walsh, Jr., and Duncan J. Maitland, "Polarized light propagation through tissue phantoms containing densely packed scatterers," Opt. Lett. **25**, 239 (2000).
19. Hiromichi Horinaka, Koji Hashimoto, Kenji Wada, Yoshio Cho, and Masahiko Osawa, "Extraction of quasi-straightforward-propagating photons from diffused light transmitting through a scattering medium by polarization modulation," Opt. Lett. **20**, 1501 (1995).
20. Y. Piederrière, J. Cariou, Y. Guern, B. Le Jeune, G. Le Brun, and J. Lortrian, "Scattering through fluids: speckle size measurement and Monte Carlo simulations close to and into the multiple scattering," Opt. Express **1**, 176 (2004). http://www.opticsexpress.org/abstract.cfm?URI=OPEX-12-1-176
21. Yasuo Hasegawa, Yukio Yamada, Mamoru Tamura, and Yasutomo Nomura, "Monte Carlo simulation of light transmission through living tissues," Appl. Opt. **30**, 4515 (1991).
22. Craig M. Gardner and A. J. Welch, "Monte Carlo simulation of light transport in tissue: unscattered absorption events," Appl. Opt. **33**, 2743 (1994).
23. Eric Tinet, Sigrid Avrillier, and Jean Michel Tualle, "Fast semianalytical Monte Carlo simulation for time-resolved light propagation in turbid media," J. Opt. Soc. Am. A **13**, 1903 (1996).
24. David A. Boas, J. P. Culver, J. J. Stott, A. K. Dunn, "Three dimensional Monte Carlo code for photon migration through complex heterogeneous media including the adult human head," Opt. Express, **10**, 159 (2002). http://www.opticsexpress.org/abstract.cfm?URI=OPEX-10-3-159
25. Akira Ishimaru, *Wave Propagation and Scattering in Random Media*, Vols. 1 and 2, Academic Press, Inc., New York (1978).
26. C. C. Yang and K. C. Yeh, "Scattering from a multiple layered random medium," J. Opt. Soc. Am. A **2**, 2112 (1985).
27. Michael S. Patterson, B. Chance, B. C. Wilson, "Time resolved reflectance and transmittance for the noninvasive measurement of tissue optical properties," Appl. Opt. **28**, 2331 (1989).

1. Introduction

The understanding of optical scattering properties is a key to the developments of efficient biological imaging techniques. By utilizing the dependencies of scattering characteristics on time, angle, and polarization, various imaging techniques have been explored. Based on backscattering, optical coherence tomography has been widely developed [e.g., 1]. Among the imaging techniques of the transmission types, both snake [2-5] and diffuse [6-8] photons have been used for efficient imaging. Here, the snake and diffuse photons are usually defined based on different photon arrival times at a detector. Although diffuse photons are more abundant and can provide higher sensitivity in imaging, the resultant spatial resolution is usually unsatisfactory. On the other hand, the techniques based on the capture of snake photons in time gating [2-5], although suffering from the low sensitivity, can provide higher resolution, in the sub-mm range. Besides capturing snake photons in time gating, the methods of angle- [9,10], aperture- [11], and polarization-gating [12-19] have been employed to utilize the coherent part of transmitted signals for imaging. In certain experiments, combination of more than one method was used for higher efficiency in imaging. Compared with the time gating technique, which usually requires a short pulse laser and a time-resolved monitoring scheme, those methods are usually less expensive.

For the studies of biological tissue imaging, phantoms, such as polystyrene micro-sphere suspension and intra-lipids, have been widely used for imitating the scattering and absorption characteristics of tissue structures. Because the effective absorption and scattering coefficients

#3820 - $15.00 US Received 13 February 2004; revised 9 March 2004; accepted 16 March 2004

of phantoms can be controlled to be quite close to those of real tissues, they have been widely applied for the development of optical imaging systems [16-18]. Meanwhile, to explore the scattering properties in biological tissues, Monte Carlo algorithms have been widely employed for simulating photon migration in a tissue sample. In such an algorithm, the concept of discrete scattering of random nature is utilized. The simulation is again based on the assumptions of effective scattering and absorption coefficients in a turbid medium [20-24].

However, recently attention has been paid to the differences in scattering properties between real tissues and phantoms [16,17]. In particular, polarization evolution is much of concern because the anisotropic properties in certain biological tissues, such as skeletal muscle and myocardium tissues, cause the optical birefringence effects. In this situation, the coherent polarization state of light is usually changed after passing through the tissues. Such coherent polarization evolution in a real tissue sample usually cannot be well simulated with a phantom in experiments or with a Monte Carlo algorithm of particle scattering nature. Actually, there exists a basic difference in general nature between phantoms and real biological tissues. Light propagation in phantoms is scattered by discrete particles in a homogenous background. Nevertheless, cells or fibers in biological tissues are arranged continuously. Although the existence of cell nuclei and walls may cause certain particle-like nature in biological tissues, the refractive index variations in a biological tissue are expected small. In other words, random continuum scattering should exist in a biological tissue. The characteristics of random continuum scattering are usually different from those of discrete scattering [25,26]. Although the effective scattering and absorption coefficients of a phantom or in a Monte Carlo simulation can describe certain photon migration characteristics, there may exist other optical scattering properties, which cannot be well described by these two parameters. However, such optical scattering properties can be quite important for optical imaging applications.

To further understand the scattering properties in biological tissues for imaging purpose, comparisons of scattering characteristics among phantoms and various biological tissues are needed. In particular, it is interesting to compare the results of various imaging techniques in applying to various samples. From the differences among different imaging techniques and different samples, features of scattering properties in different samples can be extracted. Such features can be useful for efficient imaging applications. In this paper, we measured the transmitted signals with time, aperture, and angle gating for comparison in micro-sphere suspension, skeletal muscle tissue and liver tissue. A chicken breast tissue sample was used for representing skeletal muscle tissue. Also, chicken liver tissue was used for the experiments. The different parts of the transmitted signals obtained through different gating techniques will be discussed.

This paper is organized as follows: In Section 2, the experimental procedures and sample preparations are described. The measured results of the three samples with time, aperture, angle gating are discussed in Section 3. Then, the discoveries in the combinations of time/aperture and time/angle gating are presented in Section 4. Finally, conclusions are drawn in Section 5.

2. Experimental procedures and sample preparations

Two experimental systems were built for aperture- and angle-gating measurements. In each system, time gating can always be implemented. The experiment setup for aperture gating is shown in Fig. 1. Here, a 5-W 532-nm (Coherent, Verdi-5) laser-pumped mode-locked Ti:sapphire laser (Coherent, Mirra 900) was used to provide 76 MHz, around 100 fs laser pulses at 800 nm. The laser beam was split into two branches, one for triggering the used streak camera and the other for propagating through samples. About 100-mW average power of laser pulses was applied to the samples. An adjustable aperture (A) was attached to the exit wall of the sample container or sample surface for aperture-gating measurements. It was centered at the incident laser beam axis. The transmitted signal of a sample was collected with two convex lenses (L) and then directed to the streak camera with a fiber bundle (F). The fiber bundle end was aligned with the incident laser beam. It had a receiving aperture of about 1

#3820 - $15.00 US Received 13 February 2004; revised 9 March 2004; accepted 16 March 2004

mm in diameter. The used streak camera was made by Hamamatsu with model C5680-02. Its temporal resolution was about 4 ps in the used operation mode. For aperture gating, the diameter of the smallest pinhole was 1 mm. The step size of radius increment of the pinhole was also 1 mm. Note that when the aperture is widely open (20 mm in radius), we can obtain the results of pure time gating.

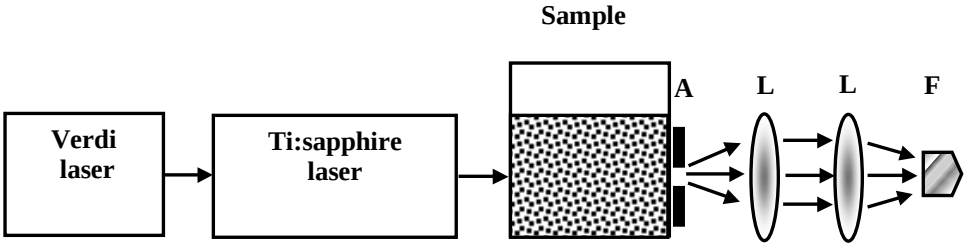

Fig. 1. Experimental setup for aperture-gating measurements. A: aperture, L: lens, F: fiber bundle connected to the streak camera.

Figure 2 shows the second experimental setup for angle-gating measurements. In this case, the fiber bundle was moved laterally with a translation stage (step size 1 mm) for varying the receiving angle. The distance between the exit wall of the sample container (or the exit surface of the sample) and the fiber bundle end was 10 cm. The angle θ is defined for describing the angle-gating measurement, as shown in Fig. 2. Because of the 10 cm distance, the results of aperture and angle gating are expected quite different.

Three different samples were prepared, including polystyrene micro-sphere suspension (sample A), fresh chicken breast tissue (sample B), and fresh chicken liver tissue (sample C). In sample A, the white polystyrene latex was diluted with water to serve as a turbid medium phantom. The average diameter of polystyrene micro-spheres (refractive index 1.565) was 1 μm. The volume concentration of diluted polystyrene suspension was 0.067 %. The suspension was contained in a plastic vessel with the transmission length of 2 cm. The chicken breast tissue sample has the thickness about 8 mm within the measurement area. The transmission length of the chicken liver sample tissue was also 8 mm. Note that the combined choices of the parameters for the micro-sphere suspension mean to result in the similar scattering strength between samples A and B (see the discussion below with Fig. 3). Although the micro-sphere size is smaller than the general dimension of biological tissues, the used micro-sphere suspension can still show useful information in scattering behavior, particularly in the comparison between the three gating methods. The same argument can be applied to the choice of the transmission length of the micro-sphere suspension. For the current consideration, the difference of transmission length between the phantom and biological tissues is not critical.

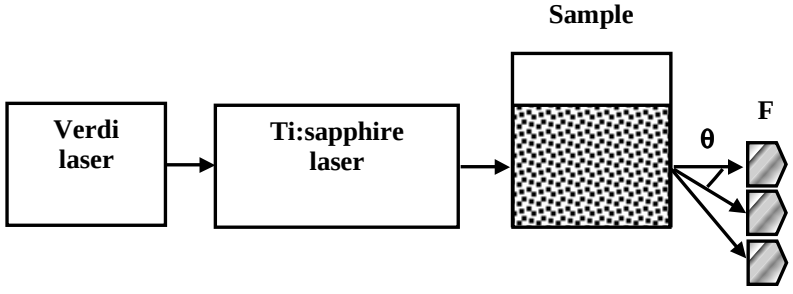

Fig. 2. Experimental setup for angle-gating measurements. F: fiber bundle connected to the streak camera.

3. Results of different samples with time, aperture, and angle gating

#3820 - $15.00 US Received 13 February 2004; revised 9 March 2004; accepted 16 March 2004

Although the major concern of this research is to compare the results of the three different gating methods, it is reasonable to first roughly compare the overall scattering behaviors between the three samples. Note that this comparison, particularly between the phantom and either biological tissue, does not mean that those samples have the same effective scattering coefficient or other parameters. Figure 3 shows time-resolved normalized intensity profiles of the three samples when the aperture in Fig. 1 is widely open. In other words, the data shown here represent the results of pure time-gating measurement. The three normalized curves are arranged such that their start-up points coincide in the time axis. Note that the log-scale curves in Fig. 3 show the two-component decay with time. They are particularly clear in the curves of samples A and B. It is usually believed that the peak position and width of a time-resolved intensity profile represent the scattering strength. Meanwhile, the profile tail is dominated by absorption [27]. In Fig. 3, one can see that samples A and B have about the same scattering strength, as designed. The curve of sample C has the largest full-width at half-maximum showing that the scattering in this sample is the strongest. Because samples B and C have the same physical length of light transmission, it is reasonable to speculate that light scattering at 800 nm in chicken liver is generally stronger than that in chicken breast tissue. From the comparison of the profile tails, one can see that the chicken liver sample has the largest absorption coefficient, followed by that of the chicken breast tissue and then that of the micro-sphere suspension.

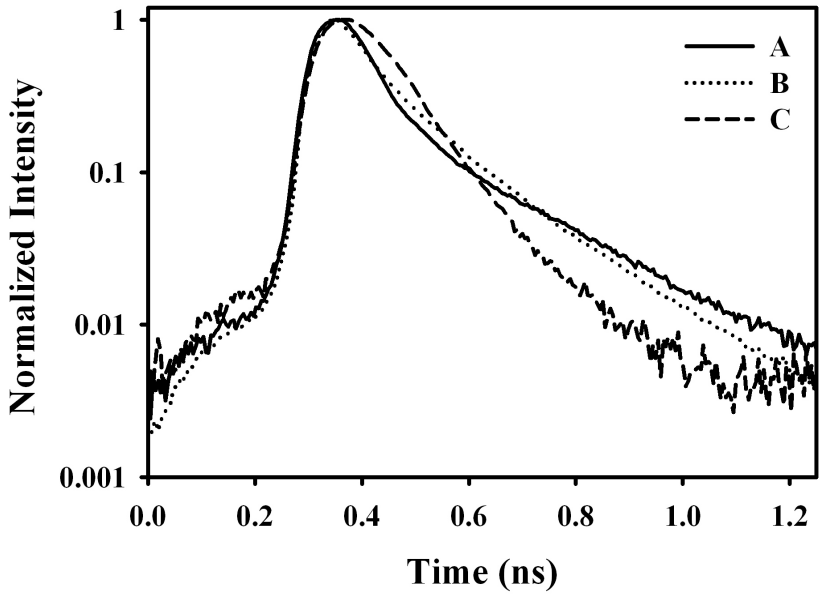

Fig. 3. Normalized intensity versus time of the three samples in the case of time gating.

In the aperture-gating measurements, different aperture sizes were used for time-resolved power measurements. The transmitted optical intensity at a radius was obtained by calculating the detected power in a ring area (obtained by subtracting the detected power of a successive smaller aperture from that of a larger aperture) and then dividing it by the ring area. In Fig. 4, the variations of normalized integrated intensity with aperture radius of the three samples are shown. The data were obtained by integrating the time-resolved intensity profiles. In other words, they are equivalent to the results of a cw laser source and represent the case of pure aperture gating. The abscissa in the figure stands for the outer radius of a ring. In Fig. 4, it is interesting to note that the aperture-gated intensity of sample A extends to larger aperture radii, when compared with those of the biological samples. One can clearly observe the relatively stronger forward-scattering characteristics in samples B and C. Although the larger-angle

#3820 - $15.00 US Received 13 February 2004; revised 9 March 2004; accepted 16 March 2004

scattering in sample A may be due to its relatively smaller particle size, the results here make us to speculate that the biological tissues contain certain nature of random continuum scattering, which mainly causes forward scattering, in contrast to the discrete nature of the phantom.

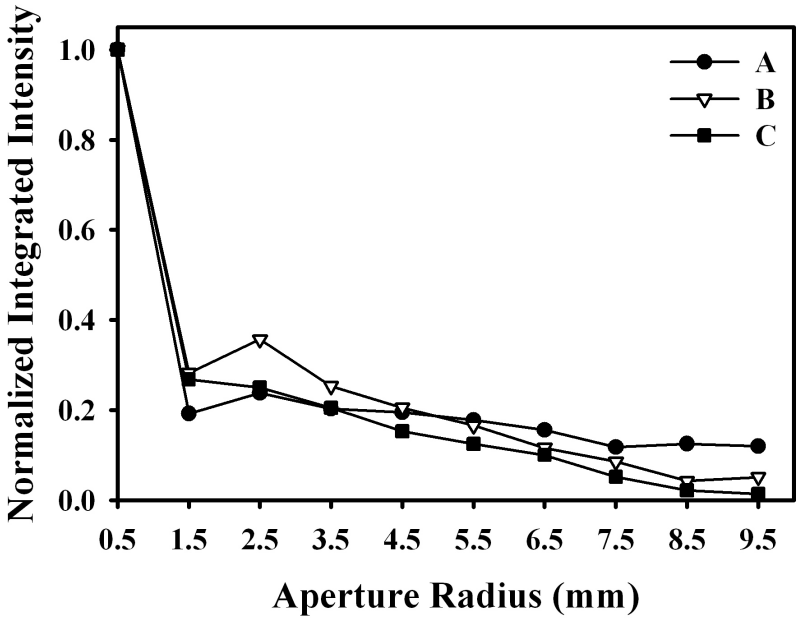

Fig. 4. Normalized integrated intensities versus aperture radius of the three samples in the case of aperture gating.

Figure 5 shows the normalized integrated intensities of transmitted signals as functions of angle θ in the angle-gating measurements for the three samples. In this figure, the upper abscissa also shows the corresponding lateral displacement of the fiber bundle end. With temporal integration, the data in Fig. 5 represent the results of pure angle gating. In principle, aperture gating is similar to angle gating. However, they actually collect not necessarily the same part of the transmitted photons. In particular, because of the 10-cm free-space propagation before signal gating in the angle gating measurement, the real angle ranges of the two gating methods are quite different. Therefore, the curve shapes in Figs. 4 and 5 are different. The most significant difference between Figs. 4 and 5 is the steep decreases of intensity from 0.5 to 1.5 mm in aperture radius (see Fig. 4), in contrast to the shallower variations of intensity with increasing angle in Fig. 5. In Fig. 5, the shallower decay of the normalized integrated intensity of sample A with angle θ indicates again the strong large-angle scattering nature. The clear forward scattering characteristics of samples B and C can also be seen in Fig. 5. This result can be attributed to either the larger cell sizes or random continuum scattering nature of this sample.

#3820 - $15.00 US Received 13 February 2004; revised 9 March 2004; accepted 16 March 2004

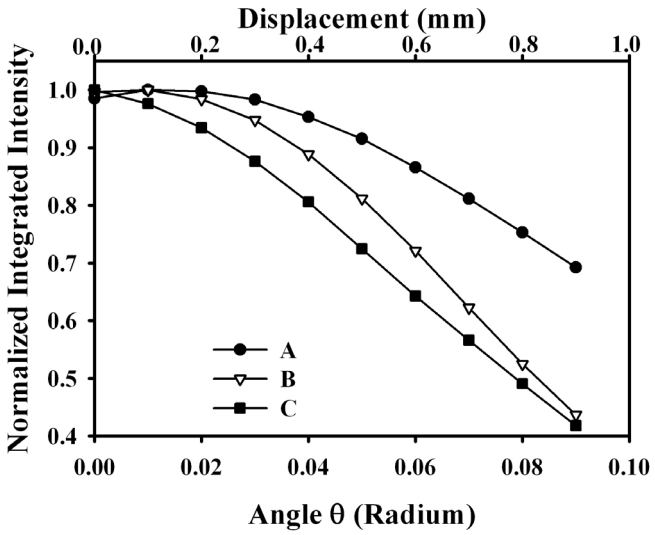

Fig. 5. Normalized integrated intensity versus angle of the three samples in the case of angle gating.

4. Combinations of time/aperture and time/angle gating

In this section, we compare the differences of detected signals between the three gating methods by combining time/aperture and time/angle gating. For easily demonstrating data, we divide the time axis into intervals and calculate the integrated intensities within intervals. Figure 6 shows the time-resolved intensity profile of transmitted signal through sample A with an aperture of 1 mm in diameter, obtained with the system in Fig. 1. The definition of the time intervals in our data process for the presentations later is illustrated with vertical dashed lines in this figure. The second and third time intervals are separated with the profile peak. The width of each interval is 47.4 ps. Note that in an individual sample with a particular gating method, the time interval definitions among different gating conditions are the same. For instance, in the aperture gating for sample A, the time interval definition is given in Fig. 6, in which the profile peak is located at the interface of the second and third intervals. The time division is the same for other aperture radii. We can do so because all the time-resolved measurements of different aperture radii have an absolute time reference, set in the used streak camera for the measurements of similar conditions. In other words, the interface of the second and third intervals will not be located at the intensity peak in the cases of larger aperture radii since the peaks are expected delayed in these cases. In aperture gating, for each sample the time intervals are always defined as Fig. 6 by the case of 1 mm in aperture radius. In angle gating, the time intervals are always defined as Fig. 6 by the case of zero radian in angle.

#3820 - $15.00 US Received 13 February 2004; revised 9 March 2004; accepted 16 March 2004

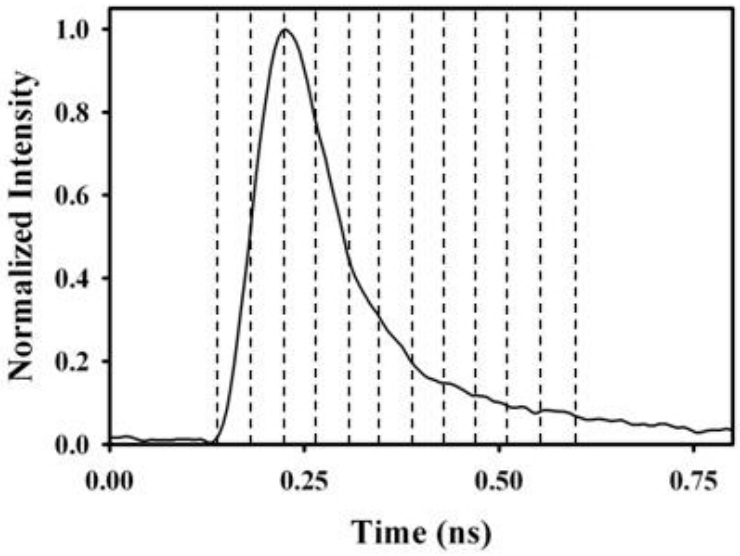

Fig. 6. Definition of time interval over the range of a time-resolved intensity profile. The second and third intervals are divided by the profile peak. Each interval width is 47.4 ps.

Figures 7-9 show the normalized intensity variations of different time intervals as functions of aperture radius for samples A-C, respectively. In each sample, the integrated intensities in the second time intervals are always the highest in a range of small aperture radius. Beyond this range, the maximum intensities appear in the third or fourth time intervals, indicating that the peak of the time-resolved intensity profile is further delayed at a larger radius. It is noted that in each of Figs. 7-9, the summation of the data point values in the curve with filled circles can be regarded as the intensity of early time gating, which is usually used for imaging purpose. Also, the summation of the data point values on the left ordinate (0.5 mm in aperture radius) can be regarded as the intensity of small aperture gating, which has been used as another means for biological imaging. Here, one can see that only part of signal from small aperture gating and early time gating overlap. In other words, in using time gating and aperture gating for imaging purposes, we actually collect different parts of transmitted signals for imaging. To see the extent of overlap, we evaluate the percentage of small aperture-gated intensity, which overlaps with early time-gated intensity. Also, we calculate the percentage of early time-gated intensity, which overlaps with small aperture-gated intensity. Such data for sample A and the other two samples are shown in Table 1.

#3820 - $15.00 US Received 13 February 2004; revised 9 March 2004; accepted 16 March 2004

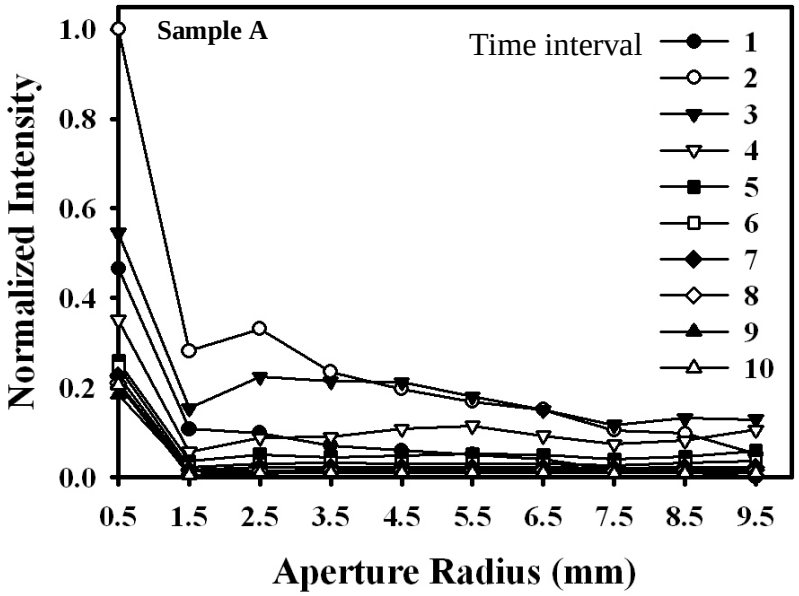

Fig. 7. Normalized intensity versus aperture radius of sample A in the case of aperture gating for different time intervals.

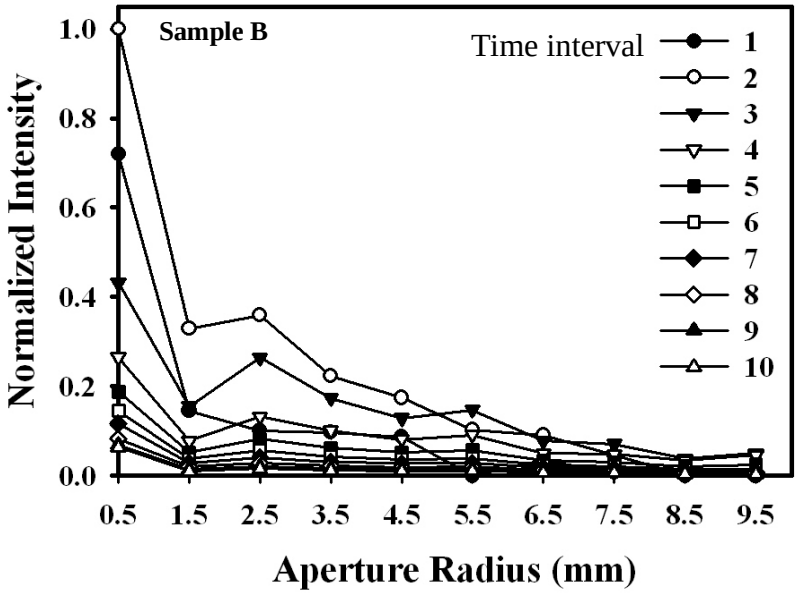

Fig. 8. Normalized intensity versus aperture radius of sample B in the case of aperture gating for different time intervals.

#3820 - $15.00 US Received 13 February 2004; revised 9 March 2004; accepted 16 March 2004

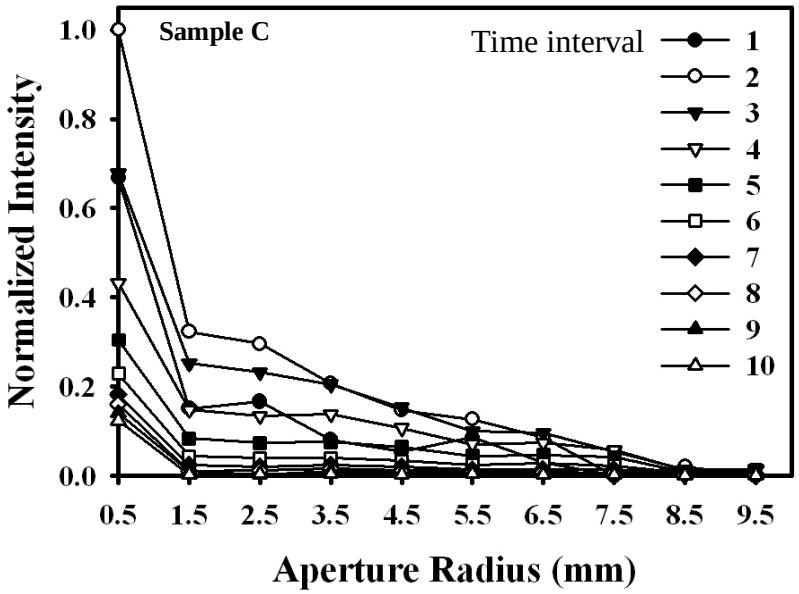

Fig. 9. Normalized intensity versus aperture radius of sample C in the case of aperture gating for different time intervals.

From Table 1, one can see that the major part of small aperture-gated signal is not covered by the early time-gated signal. However, over 50 % of the early time-gated intensity is included in the small aperture-gated intensity. This result may imply that small aperture gating collects some photons of relatively larger angle scattering. Among the three samples, the overlapping percentages are the highest in sample B (chicken breast tissue), implying the strongest forward-scattering nature in this sample.

Table 1. Overlapping percentages between the signals of different gating methods.

		Sample A	Sample B	Sample C
Aperture gating	Percentage of small aperture-gated intensity overlapping with early time-gated intensity	12.62	23.36	17.02
	Percentage of early time-gated intensity overlapping with small aperture-gated intensity	50.55	60.47	53.22
Angle gating	Percentage of small angle-gated intensity overlapping with early time-gated intensity	31.32	23.67	18.09
	Percentage of early time-gated intensity overlapping with small angle-gated intensity	18.17	16.51	17.94

Figures 10-12 show the variations of normalized intensity with angle θ in different time intervals for samples A-C, respectively. Here, one can see that in all three samples the intensity maxima shift to larger receiving angles as time increases in the range of the second to fourth time intervals (indicated with dashed arrows). This trend implies that the temporal peaks are delayed as the angle θ becomes larger, as expected. However, the extents of such shifts of intensity maximum are quite different among the three samples. The largest shifts in sample A again imply its stronger large-angle scattering.

#3820 - $15.00 US Received 13 February 2004; revised 9 March 2004; accepted 16 March 2004

Similar arguments of the overlapping signals in the combination of aperture and time gating can be applied to angle gating. In Table 1, we also show the similar overlapping percentage data between small angle-gated and early time-gated signals. Here, one can see that the signals with two gating methods do not significantly overlap. Now, sample A, instead of sample B in aperture gating, leads to the largest overlaps. This result once again shows the difference between aperture and angle-gated signals**.**

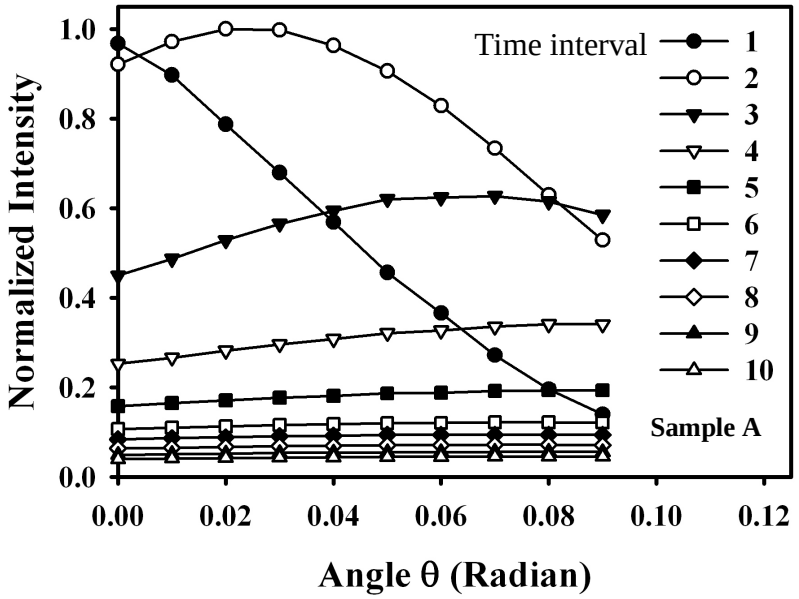

Fig. 10. Normalized intensity versus angle of sample A in the case of angle gating for different time intervals.

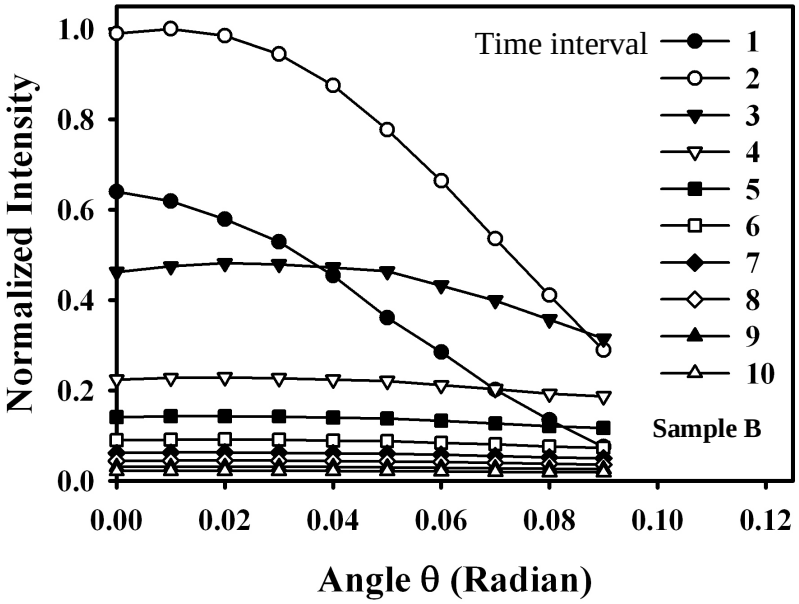

Fig. 11. Normalized intensity versus angle of sample B in the case of angle gating for different time intervals.

#3820 - $15.00 US Received 13 February 2004; revised 9 March 2004; accepted 16 March 2004

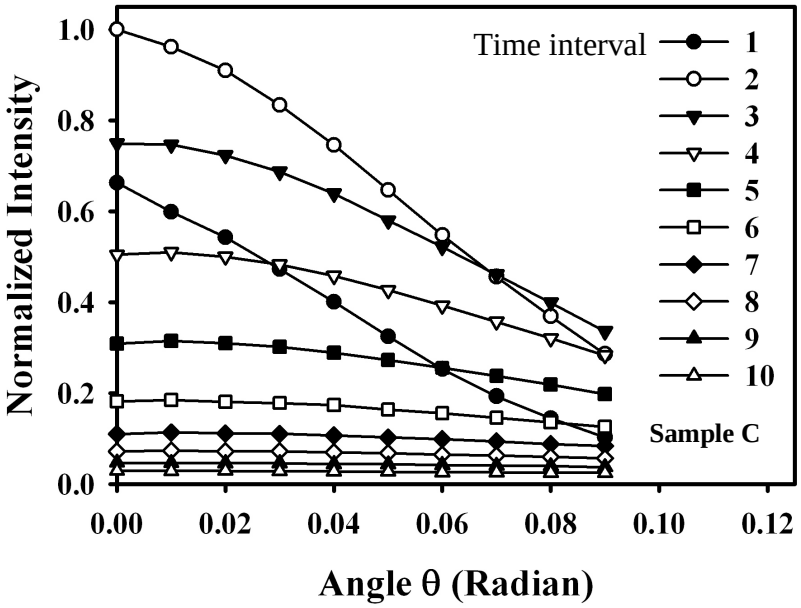

Fig. 12. Normalized intensity versus angle of sample c in the case of angle gating for different time intervals.

5. Conclusions

We have measured transmitted signals with time-, aperture-, and angle-gating for comparison in micro-sphere suspension, chicken breast and chicken liver tissues. From the data in the combinations of time/aperture and time/angle gating, we discovered that the small aperture-gated (angle-gated) signals for imaging were essentially different from those of early time-gating. Meanwhile, the signals obtained from aperture and angle gating came from quite different parts of the transmitted photons. In other words, although all the three gating methods might lead to effective biological imaging, they basically collected different portions of transmitted signals for imaging. For biological tissues of different structures, different gating methods might lead to different levels of imaging quality. It is worth exploring a most suitable gating method for a particular kind of tissue. Among the three samples, although the used micro-sphere size in the phantom is generally smaller than tissue dimensions, the rough comparisons between those samples did indicate the different scattering characteristics of biological tissues from that of a particle-based phantom. The strong forward-scattering nature in the biological tissues might imply that random continuum scattering needed to be considered in biological imaging. Between chicken breast and liver tissues, the time-gated data showed that the later had stronger scattering and absorption.

Acknowledgments

This research was supported by National Health Research Institute, The Republic of China, under the grant of NHRI-EX92-9220EI.

#3820 - $15.00 US Received 13 February 2004; revised 9 March 2004; accepted 16 March 2004